TEST CASE DOCUMENTATION
AND TESTING RESULTS

TEST CASE ID ICFD-BENCH-4.1

Galloping and fluttering

Tested with LS-DYNA® R8 Revision Beta

Tuesday 14th April, 2015

Document Information	
Confidentiality	**external use**
Document Identifier	LSTC-QA-LS-DYNA-ICFD-BENCH-4.1-1
Author(s)	Iñaki Çaldichoury, Facundo Del Pin, Rodrigo Paz
Number of pages	23
Date created	Tuesday 14^{th} April, 2015
Distribution	External

Disclaimer:

Contents

1 Introduction

1.1 Purpose of this Document

This document specifies the test case ICFD-BENCH-4.1. It provides general test case information like name and ID as well as information to the confidentiality, status, and classification of the test case.

A detailed description of the test case is given, the purpose of the test case is defined, and the tested features are named. Results and observations are stated and discussed. Testing results are provided in section 4.1 for the therein mentioned LS-DYNA® version and platforms.

2 Test Case Information

Test Case Summary	
Confidentiality	external use
Test Case Name	Galloping and fluttering: Vortex induced oscillations of buff bodies
Test Case ID	ICFD-BENCH-4.1
Test Case Status	Under consideration
Test Case Classification	Benchmarking
Metadata	FSI

Table 1: Test Case Summary

3 Test Case Specification

3.1 Test Case Purpose

The purpose of this FSI test case is to study the capabilities of the ICFD solver to solve vortex induced oscillations of rigid body spring-damper systems. A three step approach has been adopted. First, the vertical galloping motion will be studied. Next, the rotational degree of freedom will be released in order to study rotational galloping. Finally, the complete bridge fluttering problem will be analyzed. The collapse of the Tacoma Narrows bridge in 1940 reminds us of the importance of such investigations which are still the focus of a substantial body of contemporary research.

3.2 Model Description

3.2.1 Vertical Galloping

In this example, a square is immersed in a uniform flow field. It is mounted on a spring-damper support such that it can perform oscillations perpendicular to the direction of the flow (with all the other degress of freedom fixed). The channel is large enough to be regarded as infinite. Figure (1) shows the geometry of the problem. A box of finer mesh is defined around the object of interest. Different Reynolds numbers are considered. As described in [1], one characteristic behavior of this system is the 'lock in' phenomena i.e an interval of Reynolds number ($Re \approx 50-55$)) for which the vortex shedding frequency f_v coincides with the natural frequency f_n and the oscillation frequency f_0 of the square-spring system. The natural frequency can be calculated as :

$$f_n = \frac{1}{2\pi}\sqrt{\frac{k_y}{m}} \tag{1}$$

where m is the mass of the solid and k the spring stiffness.

In this 'lock-in' zone, the square performs stable oscillations. Around this interval, no oscillations occur and the vortex shedding frequency f_v starts increasing. For higher Reynolds numbers ($Re \approx 150$), the rigid body starts large amplitude oscillations and the oscillation frequency coincides with the natural frequency f_n while the vortex shedding frequency keeps increasing almost linearly. The results will be compared to those obtained by [1].

3.2.2 Rotational Galloping

In this example, the objective is to simulate the phenomena of rotational galloping. The set-up and geometry is almost identical to the vertical galloping case (see Figure(2)) except that the length of the rigid body under consideration will be varied from two to five times its thickness is order to reproduce the results by [3] (with $\Lambda = L/D$ the ratio between length and thickness and$D = 1$). The rigid body is now free to rotate but fixed in the x

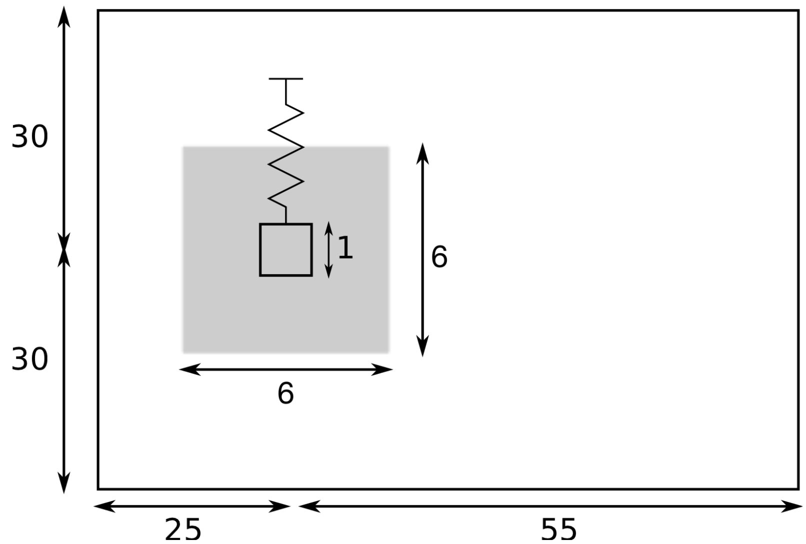

Figure 1: Test Case Sketch - Vertical Galloping

and y directions. The rotational degree of freedom is associated with an elastic spring and a certain amount of linear damping. The natural frequency can be calculated as :

$$f_n = \frac{1}{2\pi}\sqrt{\frac{k_\theta}{I_\theta}} \tag{2}$$

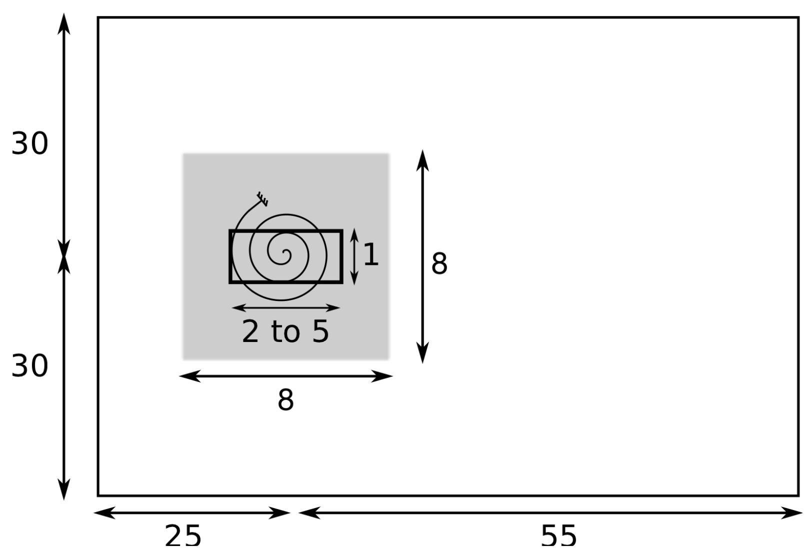

Figure 2: Test Case Sketch - Rotational Galloping

3.2.3 Bridge Fluttering

In this example, a rigid H profile bridge is considered based on the model by [2] and used in [1] (See Figure (3)). It is supported with a rotational and a vertical translation linear elastic spring. The horizontal motion is fixed to zero. The rigid body is exposed to uniform fluid flow in the horizontal direction. Bridge oscillations may consequently occur due to vertical or rotational galloping. Coupled galloping of two or more degrees of freedom is commonly known as flutter [1].

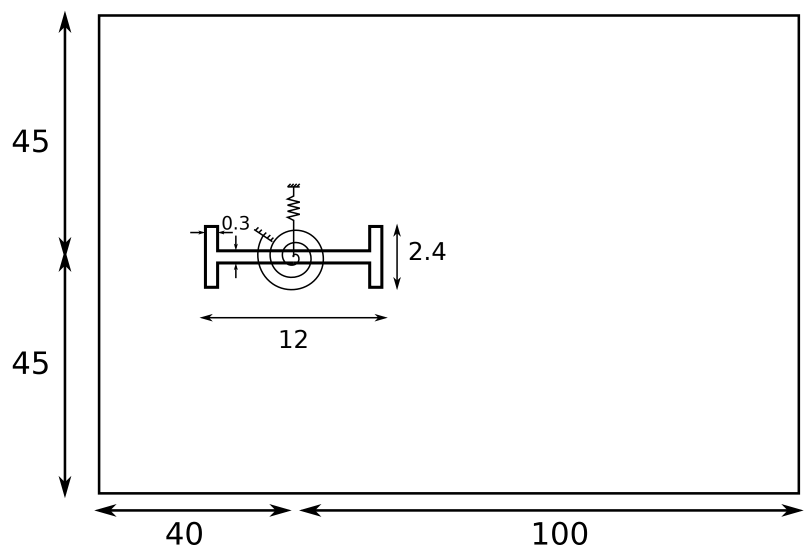

Figure 3: Test Case Sketch - Bridge Fluttering

3.3 Model Description

3.3.1 Vertical galloping

The properties of the body and the spring damper system are given in Table (2) as well as the properties of the fluid. The velocity will be varied in order to simulate a Reynolds range from 40 to 250. Figure (4) and Table (3) offer some additional information on the mesh. The mesh size has been chosen fine enough in order to consider that mesh convergence has been achieved.

Stiffness k_y	3.08425
Damping Factor c_y	0.0581195
Mass	20
Fluid Density	1
Fluid Viscosity	0.01
Time step used	0.025

Table 2: Test Case Parameters - Vertical Galloping

Model information	
Cylinder Surface Element size	0.025
Meshing Box Element size	0.05
Exterior Domain Element size	1
Elements added to the Cylinder boundary layer	2
Volume Elements	73000
Volume Nodes	36000

Table 3: Test Case Mesh - Vertical Galloping

3.3.2 Rotational galloping

The properties of the rigid body-spring system are given in Table (4). They are chosen similar to [1], with a Reynolds number $Re = u_\infty D\rho/\mu = 250$ and a natural frequency of $f_n = \sqrt{k_\theta/I_\theta}/(2\pi)) = 0.0635$ and is such a way to be able to compare with the results by [3]. Figure (5) and Table (5) offer some information on the mesh.

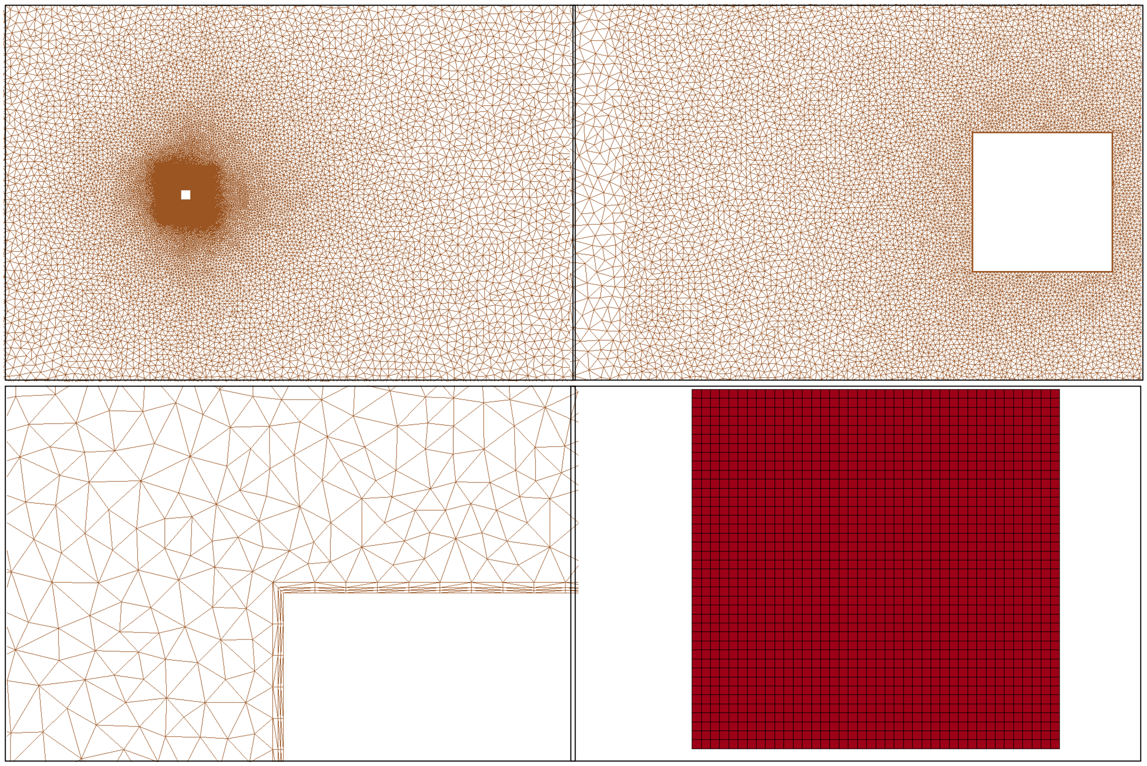

Figure 4: Overall view of the mesh, various levels of zoom on the zone close to the square and solid mesh

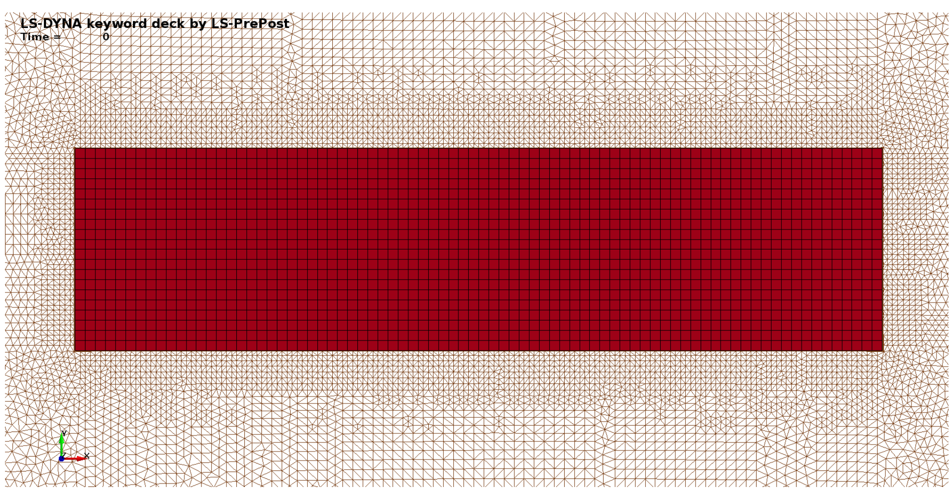

Figure 5: Overall view of the mesh for rotational galloping and $\Lambda = 4$

Inlet Velocity	2.5
Fluid Density	1
Fluid Viscosity	0.01
Time step used	0.005
$\Lambda = 2$	
Stiffness k_θ	15.4212
Damping Factor c_θ	7.854
Inertia	100
$\Lambda = 3$	
Stiffness k_θ	15.4212
Damping Factor c_θ	39.27
Inertia	100
$\Lambda = 4$	
Stiffness k_θ	61.685
Damping Factor c_θ	78.54
Inertia	400
$\Lambda = 5$	
Stiffness k_θ	61.685
Damping Factor c_θ	188.495
Inertia	400

Table 4: Test Case Parameters - Rotational Galloping

Model information	
Cylinder Surface Element size	0.025
Meshing Box Element size	0.05
Exterior Domain Element size	1
Elements added to the Cylinder boundary layer	2
Volume Elements	$\approx$ 254000
Volume Nodes	$\approx$ 127000

Table 5: Test Case Mesh - Rotational Galloping

3.3.3 Bridge fluttering

The properties of the rigid body-spring system are given in Table (6). Structural damping is ignored. Figure (6) and Table (7) offer some information on the mesh.

Stiffness k_y	2000
Stiffness k_θ	40000
Mass	3000
Intertia	25300
Inflow velocity	10
Fluid Density	1.25
Fluid Viscosity	0.1
Time step used	0.005

Table 6: Test Case Parameters - Bridge fluttering

Model information	
Bridge deck Element size	0.025
Exterior Domain Element size	1
Elements added to the boundary layer	2
Volume Elements	200000
Volume Nodes	100000

Table 7: Test Case Mesh - Bridge fluttering

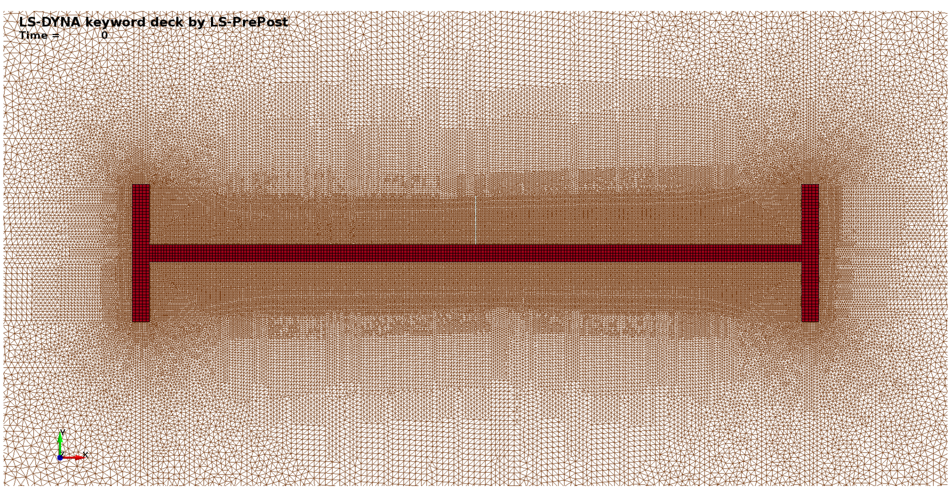

Figure 6: Overall view of the mesh for the bridge fluttering

4 Test Case Results

4.1 Vertical Galloping

Figure (7) offers a view of the Vortex shedding happening behind the square. Figure (8) and (9) show the results in the ($Re \approx 50 - 55$) region and ($Re \approx 150$) region. The lock-in phenomenon is correctly captured with an oscillation amplitude slowly decreasing from $Re = 55$ to $Re = 60$. The vortex shedding frequency is coincident with the oscillation frequency and in the vicinity of the natural frequency. After the oscillations start, both frequencies start slowly increasing. The large amplitude zone starts around $Re = 140$ which is a little bit earlier than the results by [1] where it starts around $Re = 150$. In that case, the oscillation frequency is very close to the natural frequency while the vortex shedding frequency keeps increasing. The amplitude of the oscillations also keeps increasing with a small overestimation compared to the results by [1]. On Figure (10), it can be observed that for the large amplitude zone, the oscillations reach a steady state earlier as the Reynolds number increases. Globally the results are in good agreement with the reference results of [1].

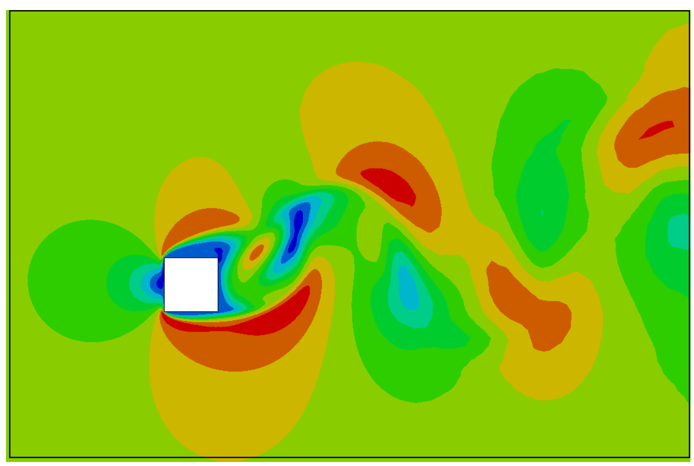

Figure 7: Test Case velocity fringes - Vertical Galloping

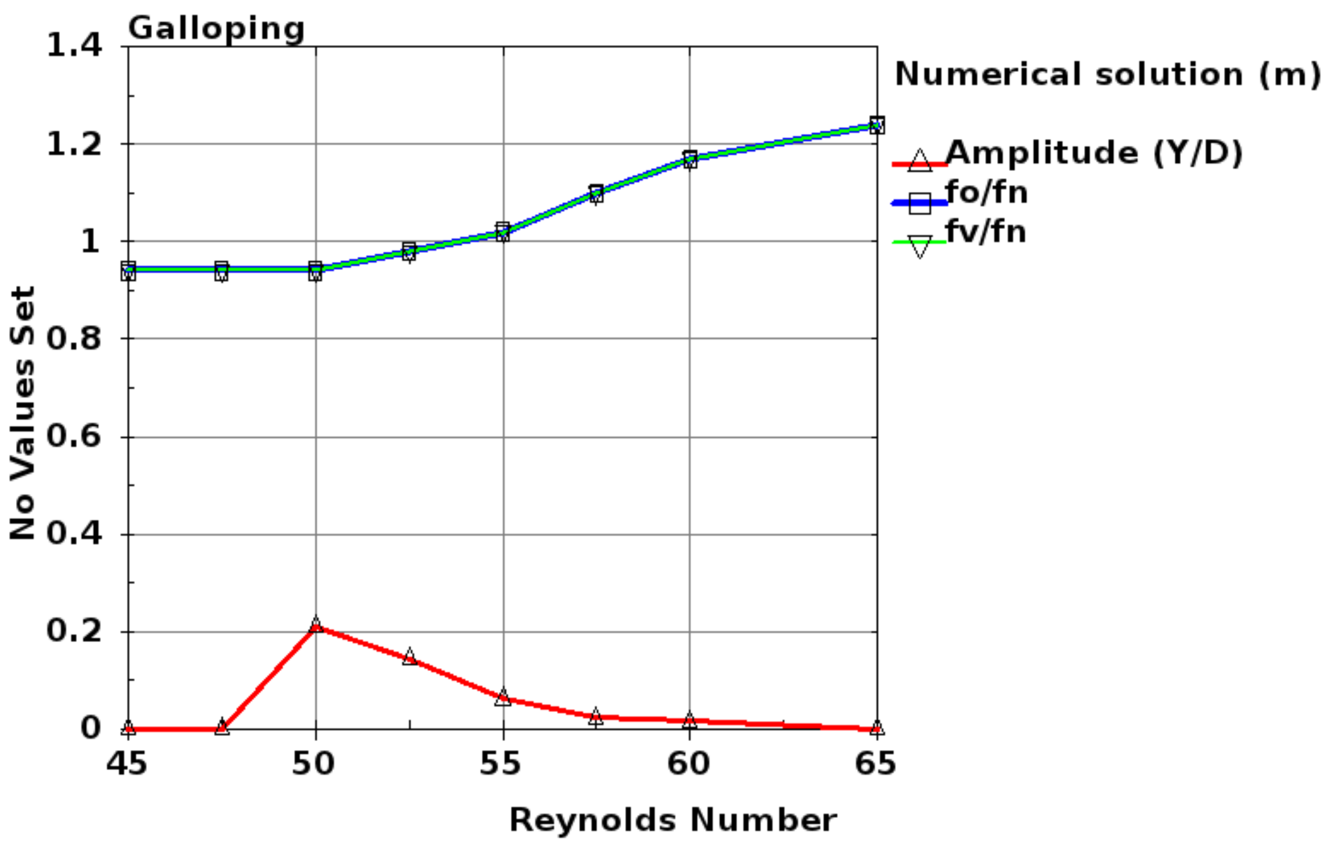

Figure 8: Test Case results regarding the Amplitude ratio (Y/D), the structure oscillation frequency f_0 and the vortex shedding frequency f_v.

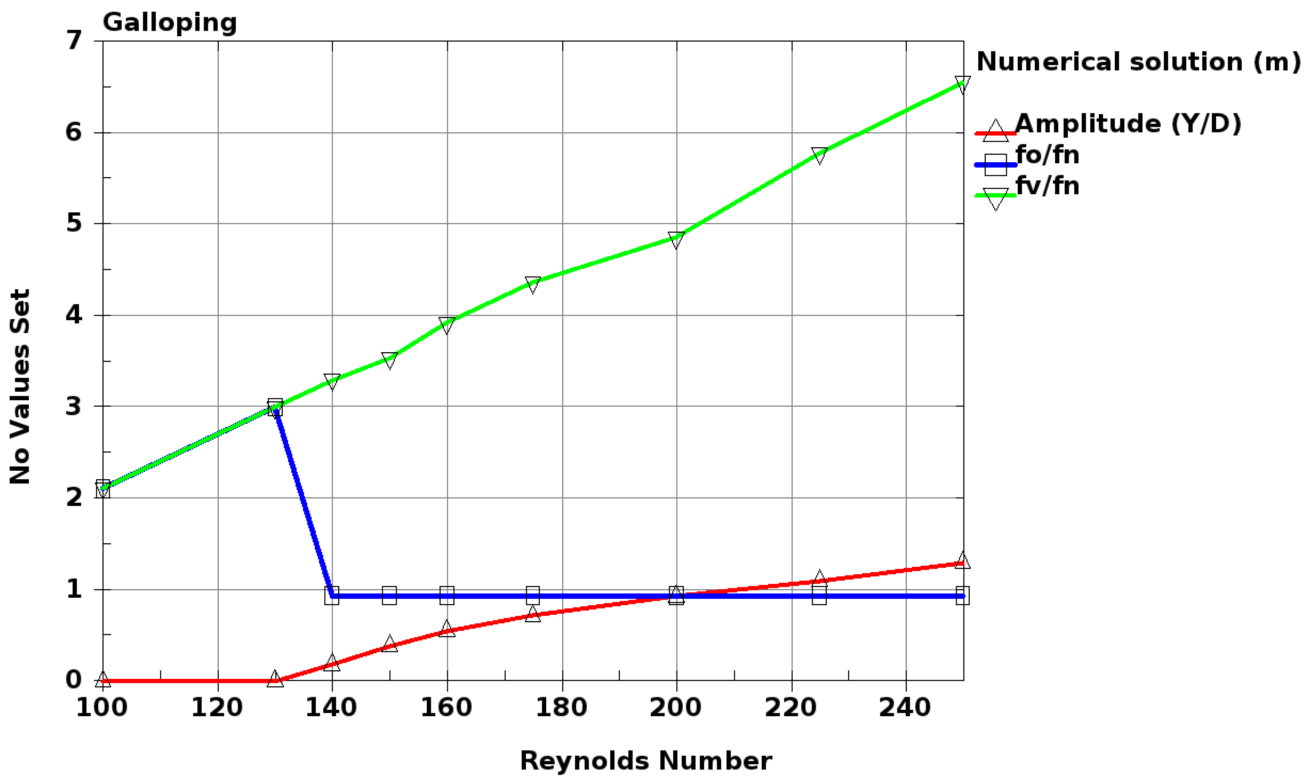

Figure 9: Test Case results regarding the Amplitude ratio (Y/D), the structure oscillation frequency f_0 and the vortex shedding frequency f_v.

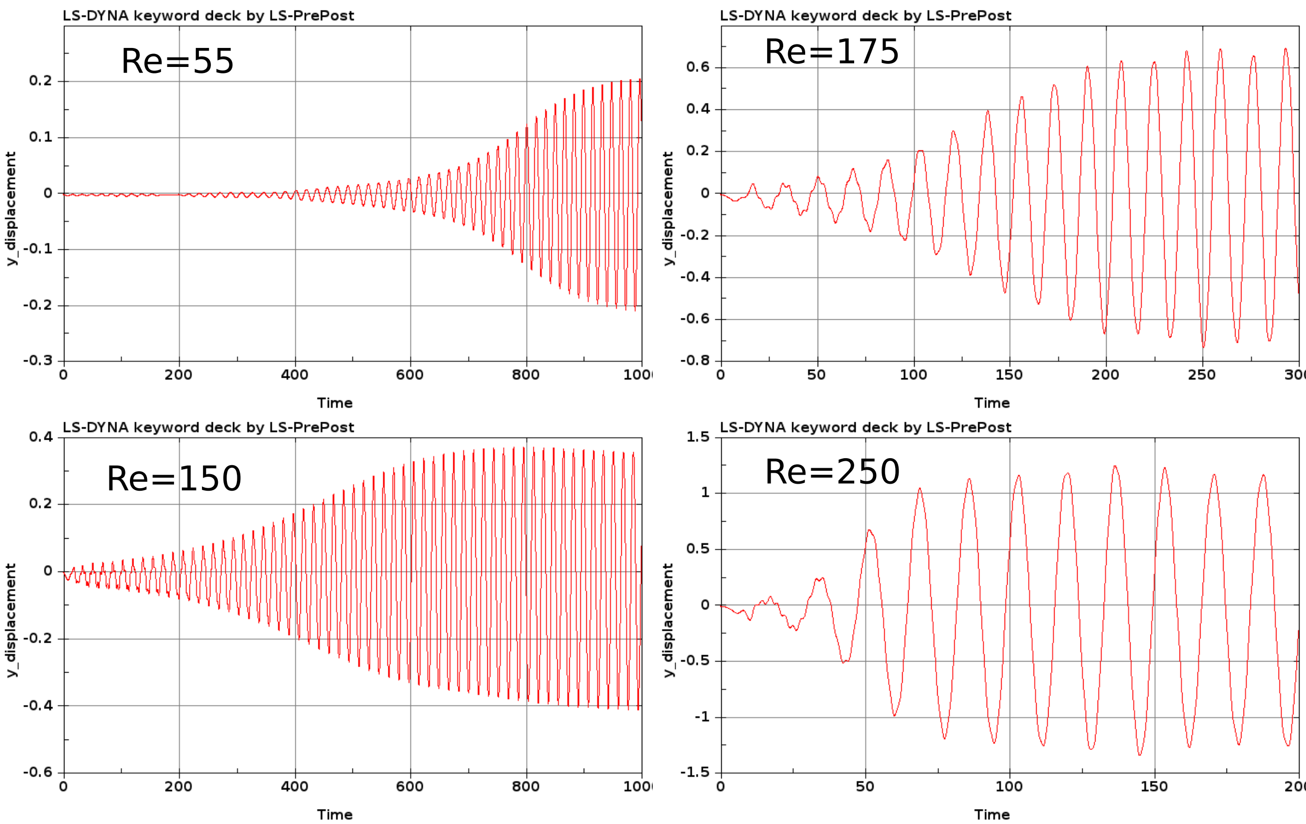

Figure 10: Behavior of the square oscillations during the transitory phase for different Reynolds numbers.

4.2 Rotational Galloping

Figure (11) offers a view of the Vortex shedding happening for $\Lambda = 4$ at two points of minimum and maximum amplitude respectfully. Figure (12), (13), (14) and (15) show the evolution of the θ rotation angle as well as the lift coefficient for the different Λ cases. The angular displacement seems to be in very good agreement with the results shown by [3] and [1]. This is further confirmed when the maximum angle and oscillation frequency is compared to the approximate values extracted from [3] in Table (8).

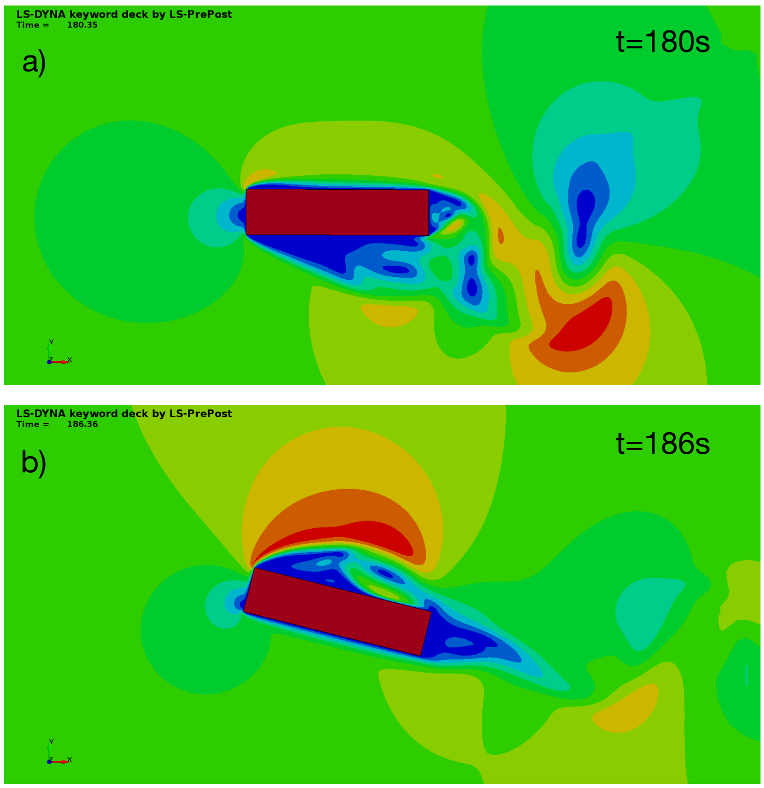

Figure 11: Test Case velocity fringes at a) $\theta \approx 0^{circ}$ and b) $\theta \approx max(\theta)$ for $\Lambda = 4$

a)
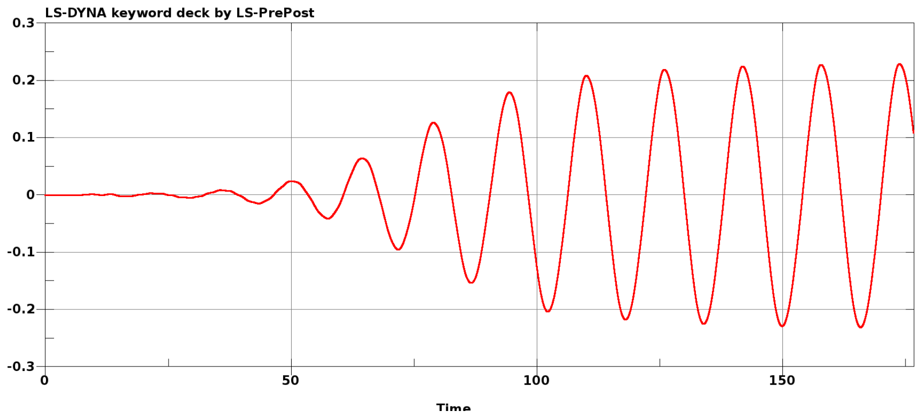

b)
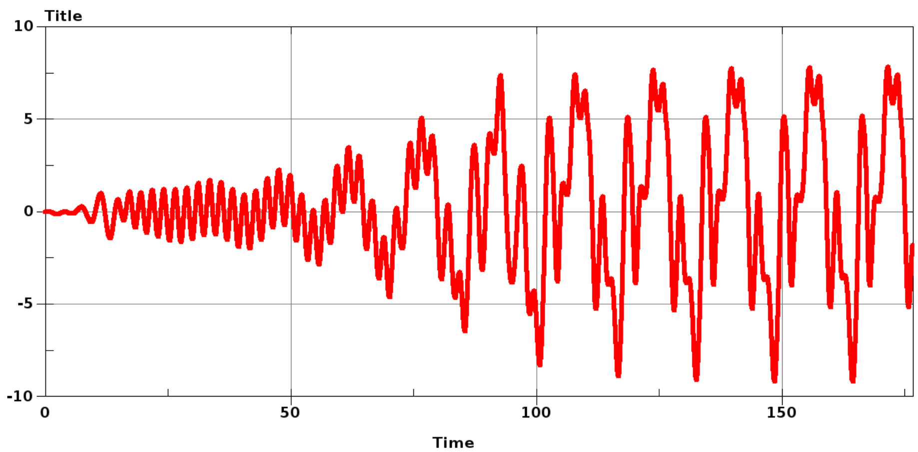

Figure 12: Rotational Galloping. Evolution of a) θ angle and of b) lift coefficient for $\Lambda = 2$

	$\Lambda = 2$		$\Lambda = 3$		$\Lambda = 4$		$\Lambda = 5$	
	$\max(\theta)$	f_o	$\max(\theta)$	f_o	$\max(\theta)$	f_o	$\max(\theta)$	f_o
Current results	0.230	0.0733	0.192	0.0488	0.248	0.0488	0.206	0.0366
Results by [3]	≈ 0.262	≈ 0.062	≈ 0.216	≈ 0.051	≈ 0.262	≈ 0.048	≈ 0.209	≈ 0.035

Table 8: Rotational galloping - Results

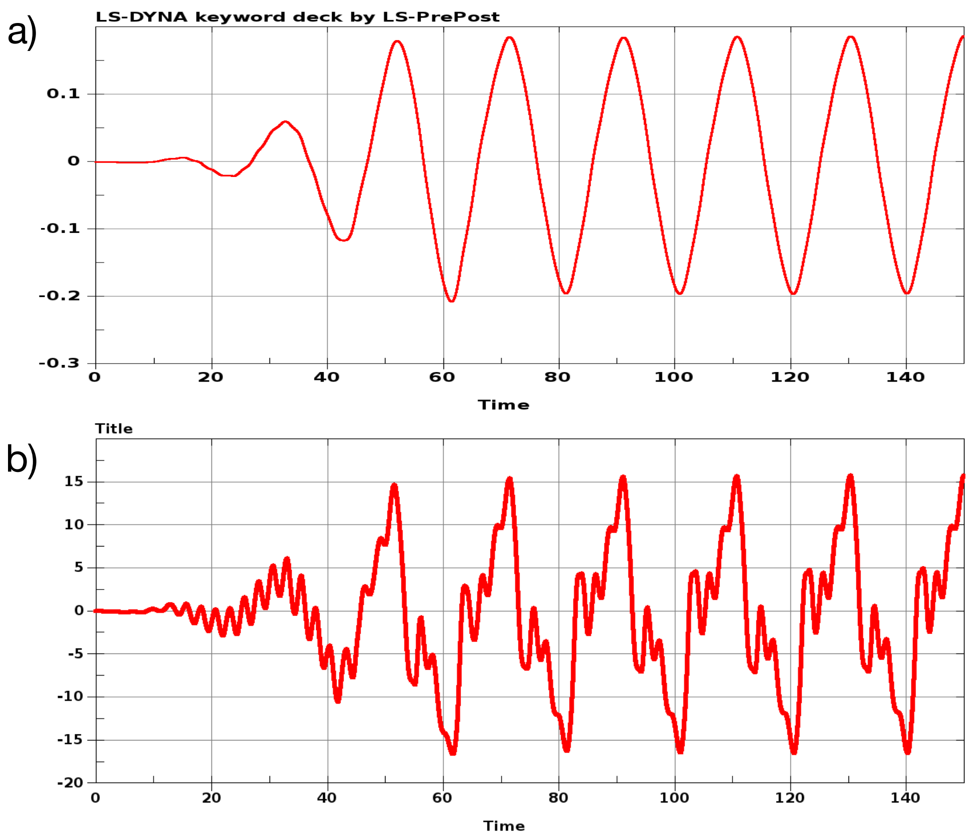

Figure 13: Rotational Galloping. Evolution of a) θ angle and of b) lift coefficient for $\Lambda = 3$

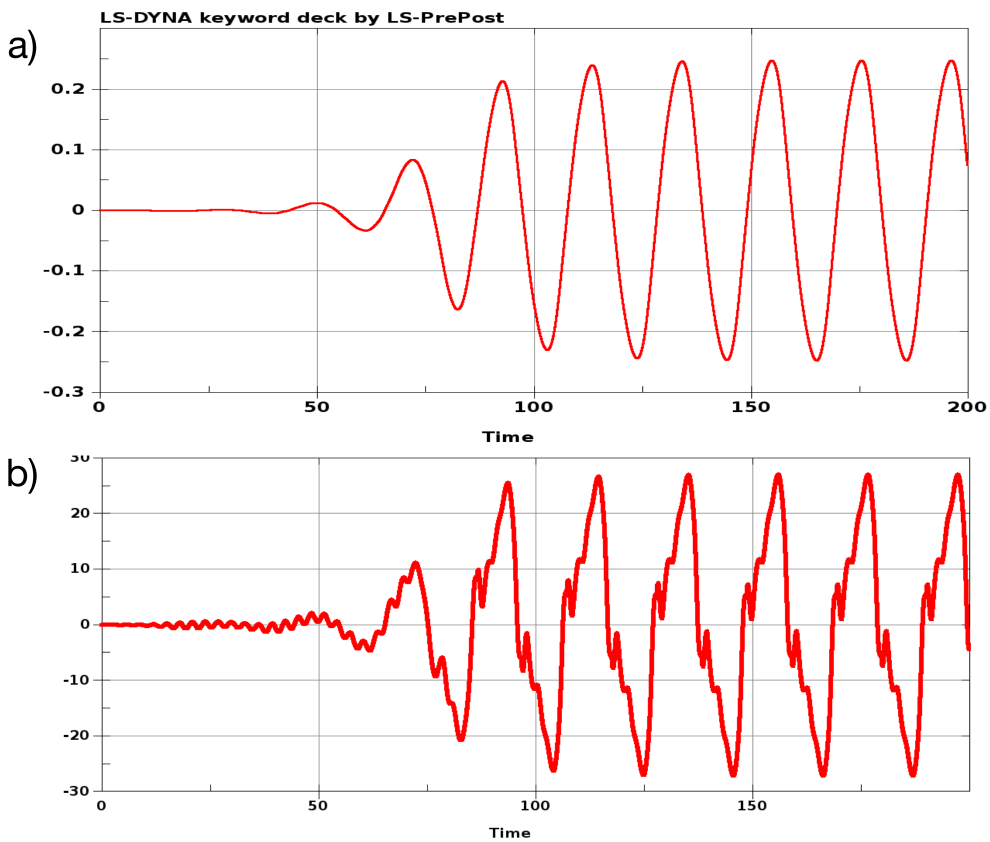

Figure 14: Rotational Galloping. Evolution of a) θ angle and of b) lift coefficient for $\Lambda = 4$

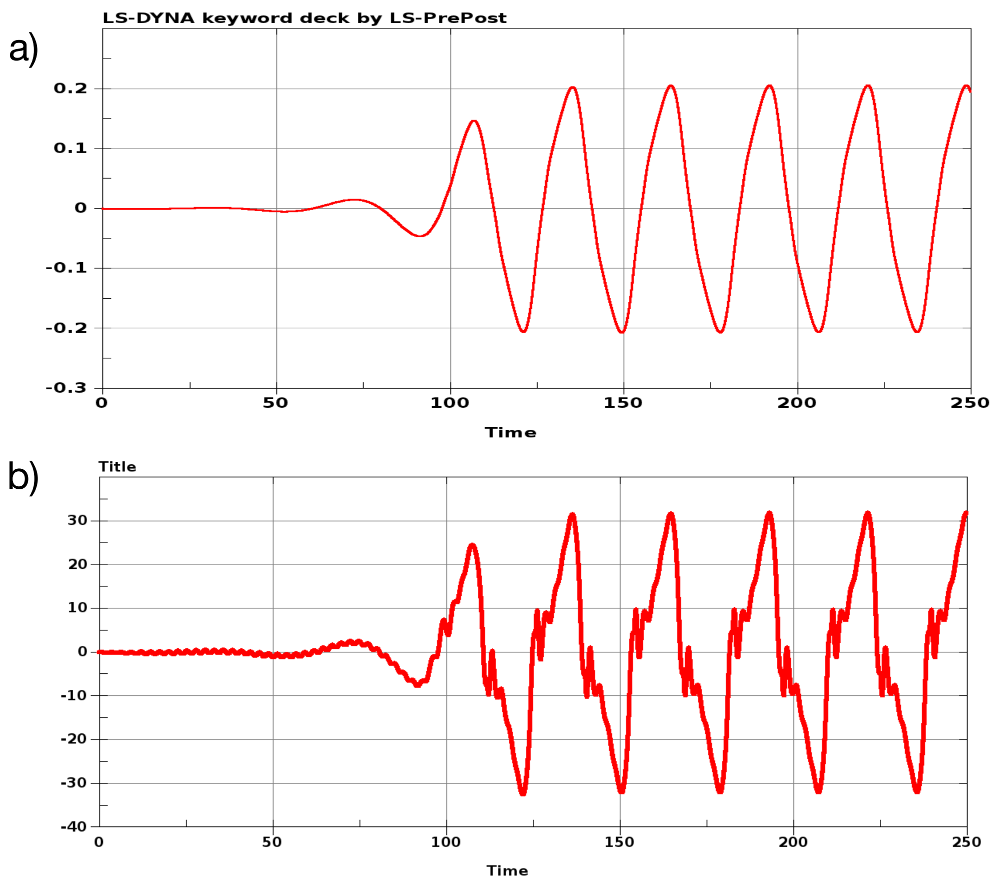

Figure 15: Rotational Galloping. Evolution of a) θ angle and of b) lift coefficient for $\Lambda = 5$

4.3 Bridge fluttering

Figure (16) shows some of the rotational motion across one period with violent angle changes over one period. It appears clearly that the rotation is the dominant motion with severe oscillations. This is further confirmed by the rotational and translation frequencies which coincide at $f_0 = 0.183s^{-1}$ which is close to the natural rotational frequency ($f_\theta = 0.200s^{-1}$ and $f_y = 0.13s^{-1}$). Figure (17) shows the establishment of the translational and rotational oscillations. The amplitude of the rotations is $max(\theta) = 57°$ and the maximum vertical displacement is obtained as $0.72 \leq max(Y) \leq 0.84$ which is again is very good agreement with the results by [1].

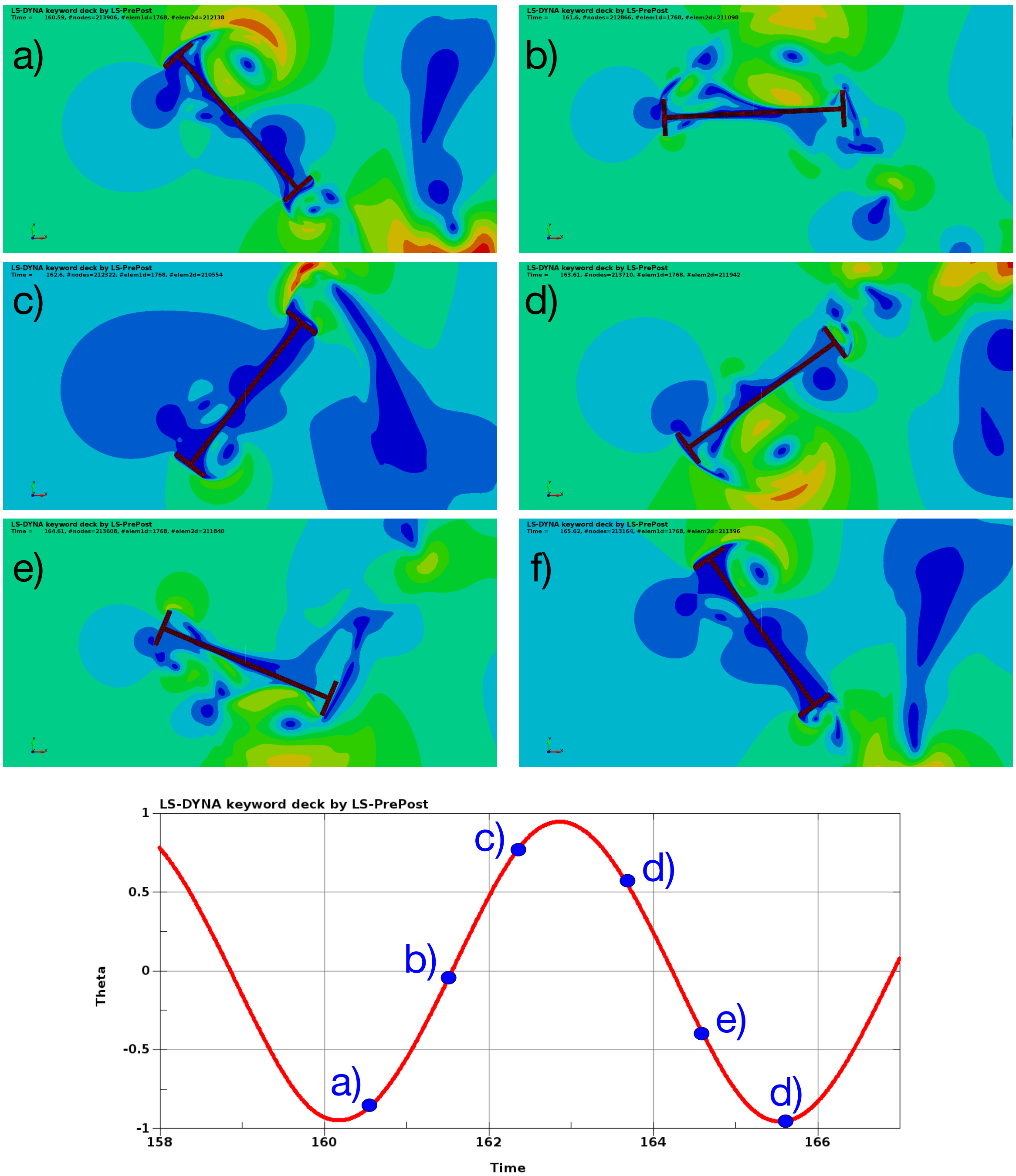

Figure 16: Flutter of the bridge deck, typical flow behavior across one period.

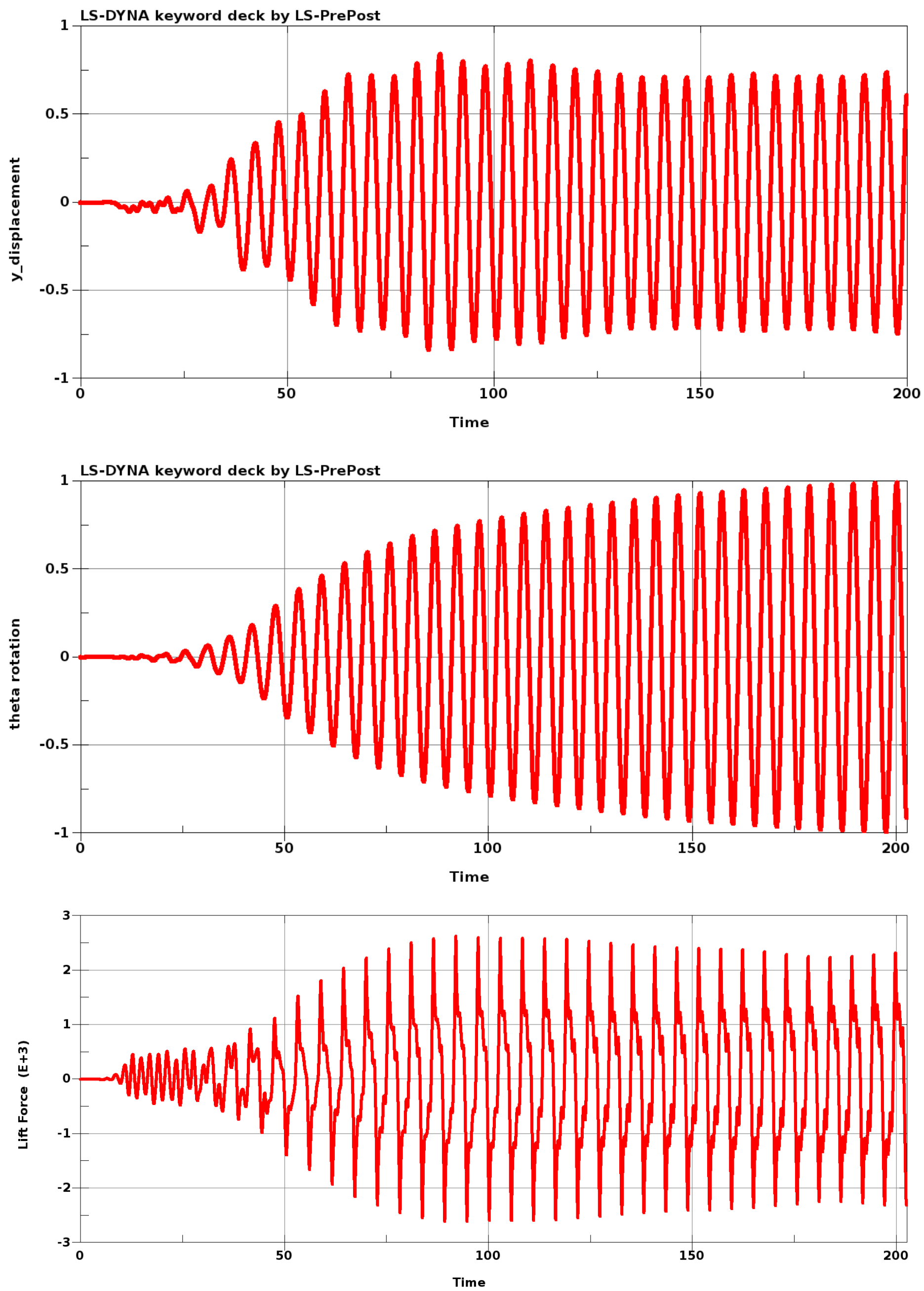

Figure 17: Flutter of the bridge deck, Y displacement, θ rotation and lift force

References

[1] W. Dettmer and D. Peric, *A computational framework for fluid-rigid body interaction: Finite element formulation and applications*, Computer methods in applied mechanics and engineering, 195 (2006), pp. 1633–1666.

[2] B. Hubner, E. Walhorn, and D. Dinkler, *Strongly coupled analysis of fluid-structure interaction using space-time finite elements*, ECCM, 2001.

[3] I. Robertson, L. Li, S. Sherwin, and P. Bearman, *A numerical study of rotational and transverse galloping rectangular bodies*, Fluids Structure, 17 (2003), pp. 681–699.